On the interface properties of ZnO/Si electroluminescent diodes

J. L. Pau,[1,a)] J. Piqueras,[1] D. J. Rogers,[2] F. Hosseini Teherani,[2] K. Minder,[3] R. McClintock,[3] and M. Razeghi[3]
[1]*Department of Applied Physics, Microelectronics Laboratory, Universidad Autónoma de Madrid, c/ Fco. Tomás y Valiente, 7, 28049 Madrid, Spain*
[2]*Nanovation, 103B Rue de Versailles, 91400 Orsay, France*
[3]*Department of Electrical Engineering and Computer Science, Center for Quantum Devices, Northwestern University, Evanston, Illinois 60201, USA*

(Received 28 September 2009; accepted 5 January 2010; published online 11 February 2010)

ZnO layers grown on n^--Si(100), n^+-Si(100), and n^--Si(111) substrates by pulsed-laser deposition were found to give electroluminescence. Light emission was observed in the form of discrete spots for currents over 1 mA with a white appearance to the naked eye. The intensity of these spots showed an erratic behavior over time, appearing and disappearing at random, while showing an associated random telegraph noise in the current signal. Regardless the substrate used, the electroluminescence spectra had a main broadband emission centered at about 600 nm and a relatively small peak at around 380 nm which corresponds to the energy of ZnO near band edge emission. Furthermore, the devices exhibited rectifying characteristics, whose current blocking direction depended on the substrate orientation. Optimization of ZnO conductivity and performing sample growth in N_2 ambient were found to be critical to enhance the emission intensity. Rutherford backscattering characterization revealed the existence of an intermixed region at the interface between ZnO and Si. To study the electronic properties at the interface, frequency dependent capacitance measurements were carried out. The junction capacitance became frequency dependent at the bias voltages at which light emission occurs due to the relatively slow trapping and generation processes at deep centers. These centers are believed to play an important role in the mechanism of light emission. © *2010 American Institute of Physics*. [doi:10.1063/1.3305530]

I. INTRODUCTION

Due to its high exciton binding energy (~60 meV) and wide bandgap (~3.34 eV), ZnO is a promising material for efficient ultraviolet (UV) emission at room temperature (RT) and beyond. Indeed, ZnO is believed to have the potential to provide emitters with higher brightness, lower threshold currents, better performance at high temperatures, and higher radiation resistance compared to their nitride-based counterparts.[1] If such devices were available, they could then be used to obtain superior white light-emitting diodes (LEDs) for solid-state lighting. To enable the fabrication of homojunction LEDs and laser diodes, considerable effort is currently being made to develop stable and reproducible *p*-type doping in ZnO.[2,3] However, it remains very difficult to obtain reliable *p*-type ZnO with sufficiently high carrier concentrations and conductivity for device applications. As a result, many reports have been limited to heterostructure *p-n* junctions.[4,5] In particular, the use of silicon substrates presents some clear advantages such as their low price, crystalline quality, easy cleaving, and potential capabilities for hybrid integration. From early investigations on ZnO materials, this substrate has been employed for the fabrication of ZnO-based piezoelectric transducers, gas sensors, and solar cell electrodes.[6–8]

Several groups have reported light emission from *n-p* and *p-n* ZnO/Si heterojunction diodes,[9–11] and recently, LEDs based on rectifying *n*-ZnO/SiO_2/*n*-Si junctions have been demonstrated.[12] A common feature of all of these studies is the observation of RT broadband visible emission. Although some have attributed the band to the radiative recombination through deep-level defects in the ZnO near the interface with the silicon, its origin is still unclear. This work aimed to gain insight on the topic through the fabrication of visible electroluminescent ZnO/Si heterojunctions grown by pulsed-laser deposition (PLD) on different *n*-type silicon substrates: n^--Si(100), n^+-Si(100), and n^--Si(111). The uniformity of the luminescence and the role of ZnO conductivity plus gas ambient during epitaxial growth were explored. Current-voltage (*I-V*) characteristics and capacitance measurements were analyzed in order to investigate the electrical properties of the heterojunction. Rutherford backscattering (RBS) was also used to study ZnO–Si intermixing at the interface.

II. EXPERIMENTAL

ZnO thin films with thicknesses of 0.7–0.8 μm were deposited on Si substrates by PLD. The deposition system comprised of a 248 nm KrF excimer laser, which irradiated a sintered ZnO target in partial N_2+O_2 ambient. For the sake of comparison, a ZnO layer was also grown on one of the substrates [n^+-Si(100)] in partial O_2 ambient. The n^--type and n^+-type silicon substrates had resistivities >20 Ω cm and <0.005 Ω cm, respectively.

The crystal structure of the as-grown ZnO layers was investigated using x-ray diffraction (XRD) with a four-circle

a)Author to whom correspondence should be addressed. Electronic mail: joseluis.pau@uam.es.

Panalytical X-Pert MRD Pro system. The surface morphology was then studied using atomic force microscopy (AFM) with a Park Scientific Instruments Autoprobe system. The optical properties were investigated using RT photoluminescence (RT-PL) spectroscopy with a frequency-doubled argon ion laser emitting at 244 nm. Hall-effect measurements were difficult for the ZnO/Si structure because the conductivity of the substrate is higher than that of the ZnO. Therefore, to prevent parallel conduction phenomena,[13] Hall-effect measurements were performed on reference layers grown on glass and sapphire substrates under the same conditions.

For device fabrication, samples were precleaned with acetone and methanol. Mesa structures with areas between 0.05 and 2 mm^2 were defined via photolithography and wet etching (1:1:50 H_3PO_4:acetic acid:H_2O). Two different kinds of top-contacts were used during this work: Pt (300 Å)/Ni (300 Å)/Au (500 Å) annealed at 600 °C for 1 min under nitrogen, and unannealed Al (1000 Å). All contacts exhibited a linear behavior due to the favorable surface properties of *n*-type ZnO for the formation of Ohmic contacts[14] The top contacts were smaller than the mesa area, leaving room for the emission of light through the uncovered surface. Finally, an Al contact was deposited on the back side of the Si. This contact was also found to be Ohmic by measuring the characteristics of two halves of the contact separated by a middle trench.

The *I-V* measurements were carried out using a probe station. To further investigate the depletion region characteristics, capacitance-voltage (*C-V*) measurements were performed (in darkness) on the devices fabricated on n^--Si(100) substrates using a HP4284A 20 Hz–1 MHz LCR meter. A Xe lamp coupled to a monochromator was used to analyze the photocapacitance under monochromatic light

In order to study the interface morphology, RBS characterization was carried out on one of the ZnO/n^--Si(100) samples by using a 5 MV terminal voltage tandem accelerator available at the Centro de Microanálisis de Materiales (CMAM) at Universidad Autónoma de Madrid (UAM). The setup was equipped with a solid-state detector held at 170°; the energy calibration of the detector was 2.62 keV/channel with an energy offset of 100 keV; the spectrum consisted of an integration over a total charge of 10 μC. The ion energy was set at 3035 keV to profit from the $O^{16}(\alpha,\alpha)O^{16}$ oxygen resonance at that energy. The experimental results were fitted using v6.04 of the "SIMNRA" program.[15]

III. PRELIMINARY MATERIAL CHARACTERIZATION

ZnO layers were characterized after growth using XRD, AFM, RT-PL, and Hall effect. The rocking curve of the ZnO (0002) reflection presented a full width at half maximum (FWHM) of about 0.84°. The AFM images showed root mean square roughnesses of about 1.5 nm and peak-to-valley values of about 9.8 nm in 1×1 μm^2 scans. Layers exhibited RT luminescence centered at 378 eV with a FWHM of about 100 meV and no evidence of the blue or yellow bands associated with N incorporation[16] and deep acceptor related defects,[17] respectively. The results shown on Fig. 1 also indicate (1) that postgrowth annealing enhances the peak intensity and (2) that samples grown in N_2+O_2 ambient show higher intensity than those grown in pure O_2. Finally, *n*-type carrier concentrations of 8.0×10^{18} and 2.5×10^{19} cm^{-3} were measured for glass and sapphire substrates with Hall mobilities of 19 and 22 $cm^2\ V^{-1}\ s^{-1}$, respectively.

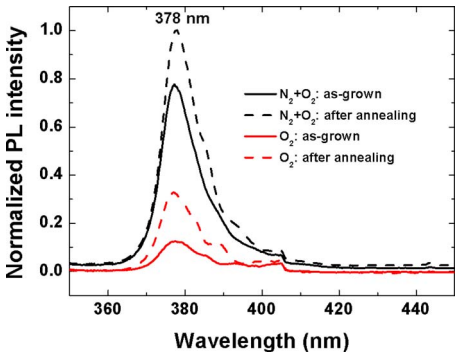

FIG. 1. (Color online) RT-PL spectra of samples grown in N_2+O_2 and O_2 ambient before (solid lines) and after (dashed lines) annealing.

IV. ELECTROLUMINESCENCE

Although several authors have reported the electroluminescence (EL) of this type of heterojunction, there is little knowledge of the uniformity of the emission. In our case, optical microscopy clearly reveals localized luminescent centers with a white appearance to the naked eye for currents over 1 mA. The bias voltages at which the light emission occurs depend on the substrate orientation and resistivity. Figure 2(a) shows the microscope image of a 0.2 mm^2 diode fabricated on the n^--Si(111) substrate taken at −20 V bias (21 mA). The picture exhibits a spot density of about $1200/mm^2$; no evidence of diode emission was found under positive bias voltages. Figure 2(b) shows the microscope image of a 0.05 mm^2 diode fabricated on the n^--Si(100) sub-

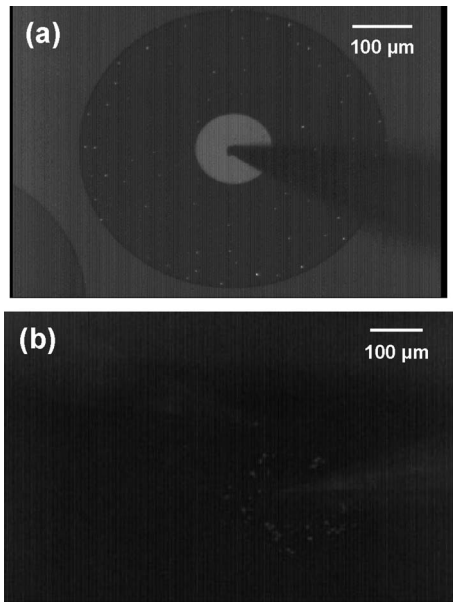

FIG. 2. (a) Microscope view of a 0.2 mm^2 area diode fabricated on n^--Si(111) at −20 V. (b) Microscope view of a 0.05 mm^2 area diode fabricated on n^--Si(100) at 14 V.

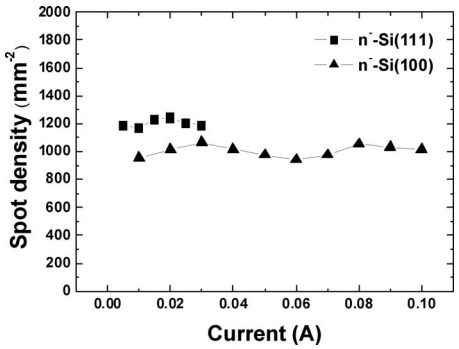

FIG. 3. Spot density vs injection current for diodes fabricated on n^--Si(111) (squares) and n^--Si(100) (triangles).

strate taken at 14 V bias (100 mA). The spot density is about 1000/mm^2; no evidence of emission was found under negative bias voltages.

The pattern of the EL showed a dependence on both time and current. Under constant bias, luminescent spots of various intensities appeared and disappeared at random over time. In some cases, new spots appeared while, in others, the same spot position extinguished and then lit up again later. The spots had various absolute intensities but the average spot brightness seemed to increase with the injected current. However, for all the devices tested, total emission power was found to be lower than 1 nW within the 1–100 mA current range. The density of spots did not appear to increase significantly with increasing current (Fig. 3). The random spot emission was also accompanied by random telegraph noise (RTS) in the current signal (Fig. 4). The amplitude of the current fluctuations varied randomly with time from about 0.2% of the total current, for the smallest fluctuations, to 7% of the current, for the largest.

The EL spectra were acquired under pulsed operation (duty cycle of 5% and frequency of 500 Hz) in order to reduce heating effects under high current injection (Fig. 5). The spectra all presented a broadband emission between 400 and 750 nm with a peak at about 600 nm. A comparable band was found for *n*-ZnO/*p*-Si diodes,[10] thus indicating that the behavior of bipolar and unipolar ZnO/Si heterojunctions is quite similar. A weaker and narrower peak, centered between about 380 and 390 nm, was also observed. Its presence was confirmed through the measurement of several diodes under different bias conditions. This emission wavelength corresponds to the near band edge (NBE) peak observed for the ZnO in photoluminescence spectra and it suggests that some carrier recombination occurred in the ZnO.

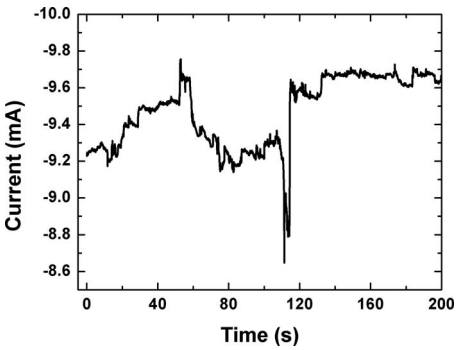

FIG. 4. Current signal of a ZnO/n^--Si(111) diode at a constant bias (−15 V).

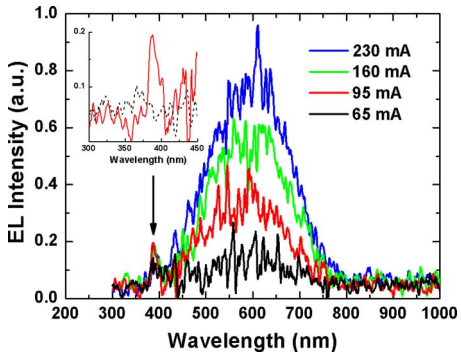

FIG. 5. (Color online) EL measurements performed in a 0.2 mm^2 area diode under pulsed operation (duty cycle of 5% and frequency of 500 Hz). The label displays the peak current values and the inset shows the weak UV emission recorded at a 95 mA peak current. Noise floor (black dashed line) obtained in absence of bias is also included in the inset as a reference.

Some devices showed localization of the emission centers in the vicinity of the metal contact pad (Fig. 6). Electrical characteristics revealed that the ZnO in such samples had higher resistivity and that the series resistance of the diodes fabricated in these areas was about twice as large than for the other diodes. Thus, it was possible that this localization of the EL could be due to reduced lateral current spreading as a result of lower conductivity of the ZnO layer.

To test the effect of the nitrogen atmosphere on device performance, devices were also fabricated on the sample grown in absence of N_2. Such samples presented up to an order of magnitude higher lateral resistivity than samples grown in N_2+O_2 ambient. Furthermore, no evidence of emission was observed from the corresponding devices, indicating that the presence of nitrogen during growth was crucial to the luminescent mechanism.

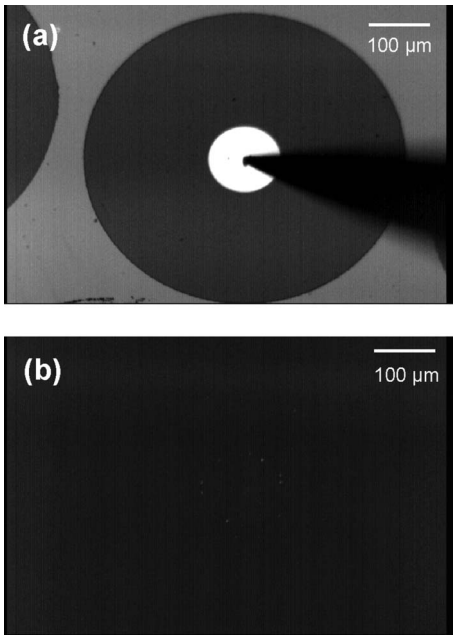

FIG. 6. (a) 0.2 mm^2 area diode fabricated on a high resistivity area of the ZnO/n^--Si(111) wafer. (b) Luminescent centers found in the same diode at −30 V (21 mA).

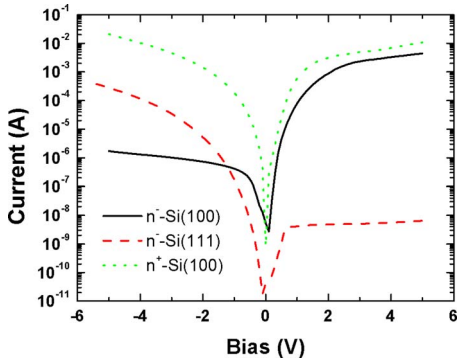

FIG. 7. (Color online) *I-V* characteristics of 0.25 mm^2 area ZnO/Si diodes fabricated on n^--Si(100), n^--Si(111), and n^+-Si(100) substrates.

V. *I-V* CHARACTERISTICS

The results of the *I-V* characterization for each substrate are illustrated in Fig. 7. Resistive substrates show a strong rectifying behavior with more than three orders of magnitude contrast between the current delivered at 5 and −5 V. A remarkable difference is noticeable between the curves obtained on n^--Si(100) and n^--Si(111) substrates. As expected from a regular *p-n* junction, the former presents high current levels at positive bias and low current levels at negative bias. In contrast, the ZnO/Si(111) devices present high current levels at negative bias and low current levels at positive bias. Since the contacts were proved to be Ohmic to ZnO and Si materials, the origin of this inverted behavior seems to be related to the different interface properties in such substrate orientation. In contrast, the measurement on a highly conductive Si(100) substrate yields a slight rectifying behavior with the same polarity as the n^--Si(100) substrate but with four orders of magnitude more leakage. Furthermore, devices fabricated on this type of substrate showed emission under positive and negative biases as a result of the high leakage currents in these diodes.

The band diagram of the heterojunction provides some insight into this behavior. The Anderson model[18] gives a conduction band offset for such structures of $\Delta E_c = \chi_{ZnO} - \chi_{Si} = 0.29$ eV, and a valence band offset of $\Delta E_V = E_{g,ZnO} - E_{g,Si} + \Delta E_C = 2.54$ eV.[9,10,12] Figure 8 illustrates the band diagram resulting from this model after using the finite element

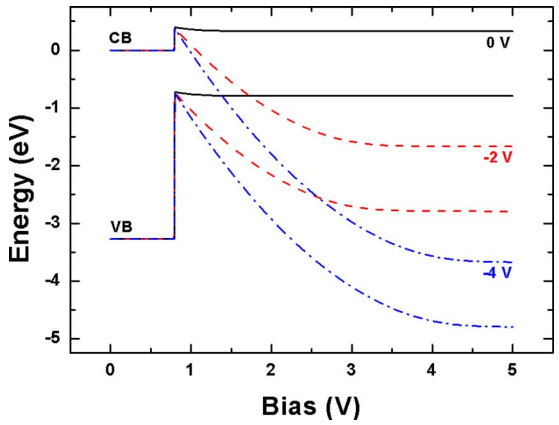

FIG. 8. (Color online) Band diagram of ZnO/Si heterojunction diodes derived from the Anderson model.

TABLE I. Extracted diode parameters for ZnO/Si heterojunction diodes fabricated on n^--Si(100). $\langle s \rangle$ and Δs represent the average value and the standard deviation, respectively.

	$\langle s \rangle$	Δs
R_s (Ω)	50	21
ϕ_B (eV)	1.7	0.1
n	2.2	0.1

method to solve the Poisson equation. Doping levels of 8×10^{18} and 3.8×10^{14} cm^{-3} were assumed for ZnO and Si, respectively. Due to the lower doping level, the voltage drop in the Si is significantly higher than the one in the ZnO, and increases with negative bias. The diagram shows a type-II alignment between Si and ZnO with a potential barrier for electrons formed by the conduction band offset. The electrons have to overcome this barrier in their flow from the ZnO to the Si at negative bias. It should be noted that the Anderson model assumes a perfectly abrupt interface, i.e., free of any intermixing between materials, and that no interface states are present.

The schematic band diagram predicts a similar behavior to that of metal-semiconductor Schottky barrier contacts and accounts for the current blocking properties of the diodes fabricated on n^--Si(100) substrates. Assuming a thermoionic emission model, the parameters of the diode fabricated on that substrate can be extracted.[19] A plot of $d(V)/d(\ln J)$ versus J will give R_sA as the slope at high current levels, where J is the current density, R_s is the series resistance, and A is the effective area of the diode. The intercept with the *y*-axis of the same plot gives nkT/q, where n is the ideality factor, q is the electronic charge, k is the Boltzmann constant, and T is the absolute temperature. To evaluate the barrier height (ϕ_B) of the diode, we can define the function $H(J)$ as

$$H(J) \equiv V - (nkT/q)\ln(J/A^{**}T^2), \tag{1}$$

where A^{**} is the Richardson constant. A plot of $H(J)$ versus J will also give a straight line with *y*-axis intercept equal to $n\phi_B$. The R_s, ϕ_B, and n calculated from the experimental data are shown in Table I. The measured barrier height is much larger than the band offset determined from the Anderson model. This result seems consistent with the existence of an interface layer with semi-insulating properties. This layer might act as a carrier blocking layer and would be responsible of the apparent discrepancy. Indeed, the high ideality factor ($n > 2$) suggests that anomalous mechanisms are involved in the electron transport through the junction.

The *I-V* characteristic for heavily doped silicon can be also explained within this framework. The tunneling current through the potential barrier becomes the dominant transport process, which is consistent with the high doping level. Consequently, the leakage increases orders of magnitude over the reverse current found for the n^--type substrate. The fitting to the *I-V* curve yields an effective barrier height of 0.61 eV.

With an inverted *I-V* curve, the devices fabricated on Si(111) do not fit the proposed model. It is known that the band offsets in heterovalent semiconductor heterojunctions depend on the atomic structure of the interface: orientation,

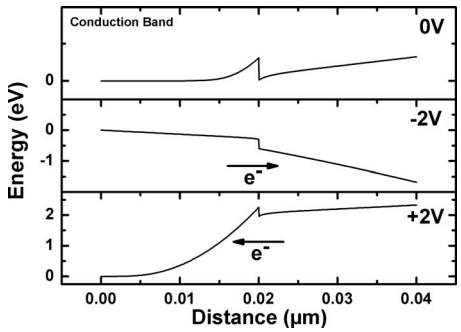

FIG. 9. Conduction band diagram of a ZnO/Si heterojunction with negative conduction band offset.

abruptness, and relaxation.[20] Thus, it is likely that the resulting conduction band offset between ZnO and Si depends on the substrate orientation and interface properties. In particular, a negative band offset would lead to a type-I heterojunction, whose potential barrier at the interface would have an opposite behavior to that found above. Figure 9 shows the conduction band diagram obtained when a conduction band offset of −0.3 eV is assumed. Under negative voltages, the electrons can flow freely from the ZnO to the Si. However, at positive biases, the electrons flowing from the Si must overcome the barrier at the interface, which limits the total current density at those voltages. Therefore, a negative band offset is a possible explanation for the inverted *I-V* characteristic of the diodes fabricated on Si(111).

VI. RBS

Figure 10(a) shows the experimental data obtained from RBS characterization. The Zn distribution results in a broadband signal at high-energies separated from the rest of the elements. Si and O signals overlap in the low-energy range of the spectrum.

Two target models were compared within the analysis: the first model consisted of a rough ZnO layer on a Si substrate (model 1); in the second model, a thin Zn–O–Si intermixed layer was added between ZnO and Si (model 2). The fitting curve and the chi-square (χ^2) test show a better agreement for model 2, due to a better fitting of the low-energy tail of the Zn band and the onset of the Si signal [Fig. 10(b)]. Table II shows the fitting parameters obtained for models 1 and 2. Despite the improved fitting, the Si signal cut-off still presents a longer tail than the simulated spectrum. This departure is caused by the preferential diffusion of Si into ZnO. The Zn–O–Si interlayer could reasonably account for this effect near the interface but fails to account for a nonuniform distribution of Si in ZnO as the ion energy increases. Assuming that the atomic density in the Zn–O–Si interlayer is the same as in ZnO (5.675 g/cm^3), and that the stoichiometry of the compound formed is $Zn_xO_xSi_y$ ($x \approx 0.25$, $y \approx 0.5$) as obtained in the fitting, a 63 nm thickness was estimated for this layer within the model 2. The non-negligible thickness and the high Si concentration found in this interlayer (48.6%) clearly alter the electrical properties of the ZnO side of the junction and might explain the semi-insulating properties of the interface found in the electrical characterization.

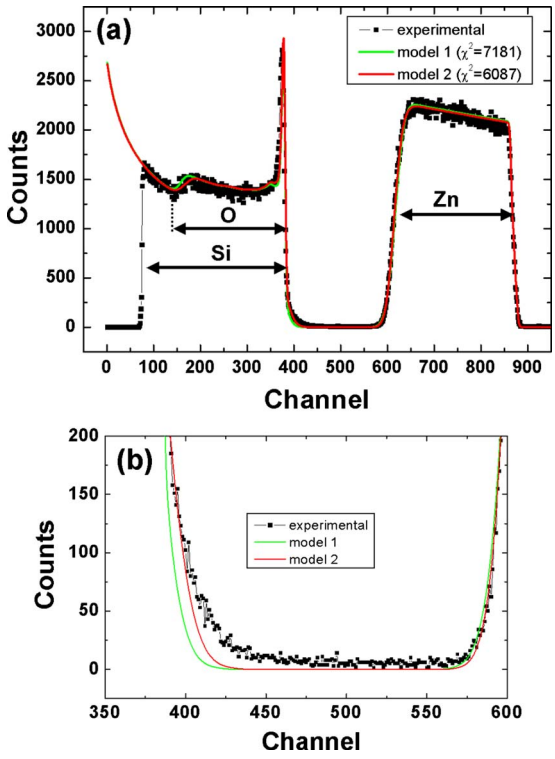

FIG. 10. (Color online) (a) RBS spectrum of a ZnO/n^--Si(100) sample. Solid lines represent the fitting results for model 1 and model 2, respectively. The calculated errors (χ^2) for each model are shown in the legend. (b) Zoom out of the region between Zn and Si signals.

VII. JUNCTION CAPACITANCE

The junction formed on resistive substrates is strongly asymmetrical: the depletion region width in the silicon is much larger than in the ZnO. Therefore, the capacitance (C) must be approximately equal to $C(V) \approx \varepsilon_{Si}/W$, where ε_{Si} is the silicon dielectric constant and W is the total depletion width. At reverse biases, the capacitance is independent of the frequency used, as shown in Fig. 11(a). However, at positive biases, for which electrons from the Si accumulate near the interface, there is a significant reduction in the capacitance with increasing frequency. Moreover, conductance rises considerably in this range of voltages. The strong reduction in capacitance with frequency is attributed to charges trapped at the interface, which cannot follow the AC signal at

TABLE II. Fitting parameters obtained for model 1 (ZnO/Si) and model 2 (ZnO/Zn–O–Si/Si). Thickness and roughness values are given in $\times 10^{15}$ atoms cm^{-2} units.

		Layer 1	Layer 2	Layer 3
Model 1	Thickness	7805	∞	⋯
	Roughness	827	⋯	⋯
	Zn (%)	47.2	0	⋯
	Si (%)	0	100	⋯
	O (%)	52.8	0	⋯
Model 2	Thickness	7181	628	∞
	Roughness	759	2.4	⋯
	Zn (%)	47.0	24.8	0
	Si (%)	0	48.6	100
	O (%)	53.0	26.6	0

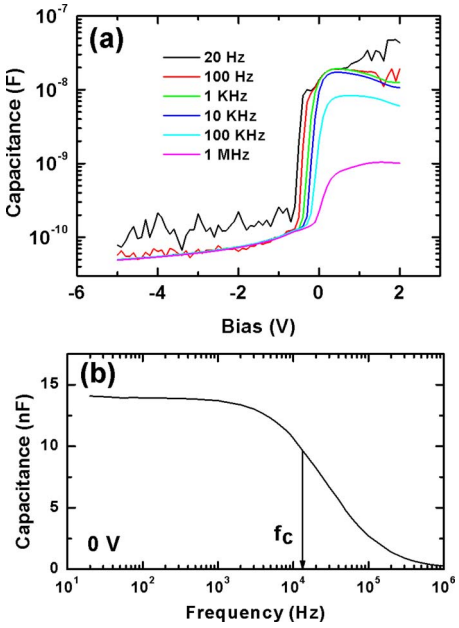

FIG. 11. (Color online) (a) *C-V* curves of a diode fabricated on a n^--Si(100) substrate at different frequencies. (b) Capacitance vs frequency.

high frequencies due to the relatively slow trapping and generation processes at deep centers. From the capacitance-frequency (*C-f*) measurements performed at zero bias, a cut-off frequency of 13.2 KHz was found—equivalent to a 12 μs time constant [Fig. 11(b)]. Therefore, taking into account that these centers will dominate the capacitance behavior at low frequencies in the range of voltages at which light emission occurs, they are believed to play an important role in the mechanism of light emission.

The $1/C^2$-*V* characteristic was linear at negative biases and quite independent of the frequency used in the 100 Hz–1 MHz range. From the $1/C^2$-*V* characteristic, a charge density of 3.7×10^{14} cm^{-3} consistent with the silicon resistivity was obtained (Fig. 12).[21] The built-in voltage (V_{bi}) was calculated from the intercept at $1/C^2=0$, yielding a value of 0.31 V. Ignoring the potential drop in the highly doped ZnO and the potential drop at the interface, which mainly depends on the resistivity of the intermixed layer, this built-in voltage would represent the potential drop in the silicon. Therefore, the conduction band offset (ΔE_c) can be calculated from the intercept voltage as follows. Assuming that the difference between the conduction band and the Fermi level is negligible

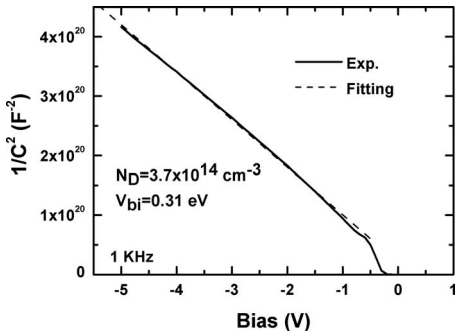

FIG. 12. Solid line: $1/C^2$ vs bias voltage at a 1 KHz frequency. Dashed line: linear fitting. The calculated values for N_D and V_{bi} are included in the graph.

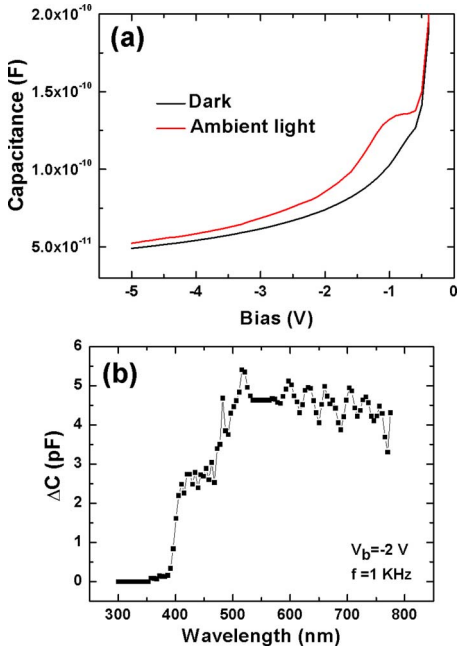

FIG. 13. (Color online) (a) *C-V* curves measured at 1 KHz in a diode fabricated on n^--Si(100) in darkness and in ambient light. (b) Photocapacitance obtained at −2 V and 1 KHz frequency.

in the ZnO, the band offset is given by $q(V_{bi}+\phi_{n,Si})$, where $\phi_{n,Si}=(kT/q)\ln(N_c/N_D)$ and represents the position of the Fermi level with respect to the conduction band in the Si; N_c and N_D are the density of states in the conduction band and the dopant density in the silicon substrate, respectively. The calculation of the band offset yields a value of $\Delta E_c=0.60$ eV, which is about twice the value predicted by the Anderson rule. However, the barrier height obtained from the *I-V* characteristic is somewhat higher due to the additional voltage drop in the intermixed layer.

In order to study the behavior of the junction under illumination, *C-V* measurements were also performed in ambient light at a frequency of 1 KHz. The *C-V* characteristic obtained is compared with the curve in darkness in Fig. 13(a). Exposure to the ambient light was observed to enhance the capacitance at reverse biases. This is a direct consequence of the photogeneration of free carriers in the depletion region and the partial screening of the electric field, which lead to the effective narrowing of the depletion region. Photocapacitance (ΔC) is defined as the difference between the capacitance under illumination and the capacitance in darkness. Figure 13(b) shows ΔC as a function of wavelength. Due to the large absorption coefficient in the ZnO, which prevents light from reaching the interface with the substrate, photons with wavelengths below 375 nm are mainly absorbed in the top layer, producing no change in the device capacitance. Thus, starting from zero at about 375 nm, the photocapacitance smoothly rises as the wavelength increases, reaching a plateau around 500 nm. In this region, the transparency of the ZnO layer enables the light with those wavelengths to go through the ZnO layer and illuminate the underlying Si. The absorbed light gives rise to the optical generation of free carriers and subsequent depletion region narrowing, which increases the device capacitance. A

similar photocapacitance spectrum has been reported in *n*-ZnO/*p*-Si heterojunctions under negative voltages,[22] which again shows the similar performance of bipolar and unipolar devices.

VIII. CONCLUSIONS

In conclusion, ZnO thin films were grown on n^--Si(100), n^+-Si(100), and n^--Si(111) substrates by PLD for the study of ZnO/Si electroluminescent diodes. The EL was observable for currents over 1 mA and emanated from discrete spots. Localization of the EL around the electrodes in more resistive samples suggested that the ZnO layer plays the role of a current spreading layer. Experiments on samples grown in the absence of nitrogen showed no light emission. The spectral analysis revealed a broadband EL with a main peak around 600 nm and a small peak at the ZnO NBE.

ZnO/Si diodes exhibited rectifying *I-V* curves whose polarization depended on the substrate orientation. ZnO/Si(100) diodes behaved as type-II heterojunctions, whereas ZnO/Si(111) behaved as type-I heterojunctions. Highly doped substrates yielded high leakage currents due to the tunneling contribution through the interface barrier. RBS characterization demonstrated the existence of an intermixed region at the interface with preferential diffusion of Si toward the ZnO layer.

Junction capacitance was highly dependent on frequency under carrier accumulation near the interface and it was sensitive to radiation with photons of lower energy than the ZnO bandgap.

ACKNOWLEDGMENTS

The authors would like to thank E. Ruiz, M. Cervera, and the UAM personnel of CMAM for his help with device fabrication, capacitance measurements, and RBS characterization. They also acknowledge the Spanish Ministry of Education and Science for supporting one of the authors through the "Ramón y Cajal" Program (J. L. P.).

[1] D. C. Look, Mater. Sci. Eng., B **80**, 383 (2001).
[2] K.-K. Kim, H.-S. Kim, D.-K. Hwang, J.-H. Lim, and S.-J. Park, Appl. Phys. Lett. **83**, 63 (2003).
[3] A. Tsukazaki, A. Ohtomo, T. Onuma, M. Ohtani, T. Makino, M. Sumiya, K. Ohtani, S. F. Chichibu, S. Fuke, Y. Segawa, H. Ohno, H. Koinuma, and M. Kawasaki, Nature Mater. **4**, 42 (2005).
[4] Ya. I. Alivov, J. E. Van Nostrand, D. C. Look, M. V. Chukichev, and B. M. Ataev, Appl. Phys. Lett. **83**, 2943 (2003).
[5] A. Osinsky, J. W. Dong, M. Z. Kauser, B. Hertog, A. M. Dabiran, P. P. Chow, S. J. Pearton, O. Lopatiuk, and L. Chernyak, Appl. Phys. Lett. **85**, 4272 (2004).
[6] A. S. Khan and A. Ambardar, J. Mater. Sci. Lett. **2**, 789 (1983).
[7] V. I. Anisimkim, M. Penza, A. Valentini, F. Quaranta, and L. Vasanelli, Sens. Actuators B **23**, 197 (1995).
[8] D. G. Baik and S. M. Cho, Thin Solid Films **354**, 227 (1999).
[9] X. Li, B. Zhang, H. Zhu, X. Dong, X. Xia, Y. Cui, Y. Ma, and G. Du, J. Phys. D: Appl. Phys. **41**, 035101 (2008).
[10] J. D. Ye, S. L. Gu, S. M. Zhu, W. Liu, S. M. Liu, R. Zhang, Y. Shi, and Y. D. Zheng, Appl. Phys. Lett. **88**, 182112 (2006).
[11] L. J. Mandalapu, Z. Yang, S. Chu, and J. L. Liu, Appl. Phys. Lett. **92**, 122101 (2008).
[12] S. T. Tan, X. W. Sun, J. L. Zhao, S. Iwan, Z. H. Cen, T. P. Chen, J. D. Ye, G. Q. Lo, D. L. Kwong, and K. L. Teo, Appl. Phys. Lett. **93**, 013506 (2008).
[13] J.-L. Zhao, X.-M. Li, A. Krtschil, A. Krost, W.-D. Yu, Y.-W. Zhang, Y.-F. Gu, and X.-D. Gao, Appl. Phys. Lett. **90**, 062118 (2007).
[14] K. Ip, G. T. Thaler, H. Yang, S. Y. Han, Y. Li, D. P. Norton, S. J. Pearton, S. Jang, and F. Ren, J. Cryst. Growth **287**, 149 (2006).
[15] M. Mayer, Report No. IPP 9/113, Max Planck Institut Garching, Germany, 1997.
[16] D. J. Rogers, D. C. Look, F. Hosseini Téhérani, K. Minder, M. Razeghi, A. Largeteau, G. Demazeau, J. Morrod, K. A. Prior, A. Lusson, and S. Hassani, Phys. Status Solidi C **5**, 3084 (2008).
[17] M. A. Reshchikov, V. Avrutin, N. Izyumskaya, R. Shimada, and H. Morkoc, Physica B **401–402**, 374 (2007).
[18] R. L. Anderson, IBM J. Res. Dev. **4**, 283 (1960).
[19] S. K. Cheung and N. W. Cheung, Appl. Phys. Lett. **49**, 85 (1986).
[20] M. Peressi, N. Binggeli, and A. Baldereschi, J. Phys. D: Appl. Phys. D **31**, 1273 (1998).
[21] S. M. Sze, *Physics of Semiconductor Devices* (Wiley, New York, 1981), Chap. 1, p. 32.
[22] S. Mridha and D. Basak, J. Appl. Phys. **101**, 083102 (2007).